Unconventional full-gap superconductivity in Kondo lattice with semimetallic conduction bands

Shoma Iimura,[1] Motoaki Hirayama,[2] and Shintaro Hoshino[1]
[1]*Department of Physics, Saitama University, Shimo-Okubo, Saitama 338-8570, Japan*
[2]*RIKEN Center for Emergent Matter Science (CEMS), Wako, Saitama 351-0198, Japan*

(Received 19 November 2018; revised manuscript received 19 July 2019; published 30 September 2019)

A mechanism of superconductivity is proposed for the Kondo lattice which has semimetallic conduction bands with electron and hole Fermi surfaces. At high temperatures, the f electron's localized spins/pseudospins are fluctuating between electron and hole Fermi surfaces to seek for a partner to couple with. This system tries to resolve this frustration at low temperatures and chooses to construct a quantum mechanically entangled state composed of the Kondo singlet with electron surface and that with hole surface, to break the U(1) gauge symmetry. The corresponding order parameter is given by a composite pairing amplitude as a three-body bound state of localized spin/pseudospin, electron and hole. The electromagnetic response is considered, where the composite pair itself does not contribute to the Meissner effect, but the induced pair between conduction electrons, which inevitably mixes due to, e.g., a band cutoff effect at high energies, carries the superconducting current under the external field. Possible applications to real heavy-electron materials are also discussed.

DOI: 10.1103/PhysRevB.100.094532

I. INTRODUCTION

The mechanism of unconventional superconductivities is an important issue in condensed matter physics [1–3] in designing a guiding principle to find new superconductors. The superconducting materials range over a broad class of correlated electron materials including cuprates, iron pnictides, and organic compounds [4]. Among them, the heavy electron materials with nearly localized f electrons are typical systems showing unconventional superconductivity, and the identification of the mechanisms has still remained open question since the discovery of $CeCu_2Si_2$ [1] and UBe_{13} [5] in lanthanide- and actinide-based materials. Whereas the recent advanced experiments allow to determine the symmetry or structure of pairing gap functions, the underlying mechanisms have not yet been fully clarified.

Recently, specific heat measurements in a rotating magnetic field have revealed the full-gap nature of the superconducting states in $CeCu_2Si_2$ [6] and UBe_{13} [7], in addition to a well known cerium-based s-wave superconductor $CeRu_2$ [8]. This is in contrast with the conventional notion that the strongly correlated electrons favor a spatially nonlocal and anisotropic pairing. Hence, it is desirable to identify a new mechanism for full-gap superconductivity that is specific to heavy-electron materials. To this end, we here focus on the physics arising from a semimetallic band structure having both electron and hole Fermi surfaces. One of the characteristics of the correlated semimetal is an emergence of excitonic insulator [9–11], where the Coulomb interactions reconstruct the electronic states near the Fermi level and form a gap at the Fermi level. Another interesting problem, which is discussed in this paper, is to consider the situation where the semimetal interacts quantum-mechanically with magnetic ions through the antiferromagnetic Kondo coupling as illustrated in Fig. 1.

We show in this paper that the Kondo lattice with semimetallic conduction bands exhibits a full-gap superconductivity as a consequence of resolution of a frustration associated with the multichannel Kondo effect. Underlying physical picture is the following: at high temperatures electron and hole bands are competing in screening the localized moments (see Fig. 1), and at low temperatures they decide to mix the two kinds of Kondo singlet states quantum-mechanically. As a result, the electrons and holes are superposed and superconductivity occurs since the U(1) gauge symmetry is broken. The resultant order parameter is the composite pair amplitude [12–15], which has been proposed in the multichannel Kondo/Anderson lattices [16–24]. A new perspective proposed here is that the stability of this composite pairing is closely related to the semimetallic conduction bands. The mechanism is also related closely to the concept of frustration. It has been argued that the frustration generates intriguing quantum states out of classically degenerate states. The well-known example is the spin liquid caused by the geometrical frustration in the magnetically interacting systems [25,26]. In our setup, the frustration arises in the form of the competing screening channels in Kondo systems, which is resolved by utilizing the quantum states, and even realizes the gauge-symmetry broken state.

For theoretical analysis, we take the parabolic dispersion for conduction electrons, which makes the physical picture clear with a *pure* composite pairing state without conventional one-body pair amplitudes. The electromagnetic response is also considered based on the microscopic Hamiltonian, and the pure composite pair does not directly couple to electromagnetic field in linear response. Instead, with the consideration of lattice regularization (or band cutoff effect) that modifies the parabolic dispersions far away from Fermi surfaces, a usual one-body pair amplitude is secondarily induced and then show electromagnetic linear-response.

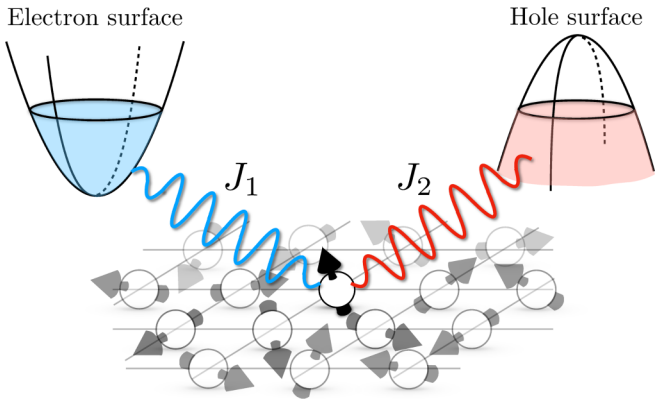

FIG. 1. Schematic picture for pairing in Kondo lattice with semimetallic conduction bands.

II. KONDO LATTICE WITH SEMIMETALLIC CONDUCTION BANDS

We use the following Hamiltonian for the Kondo lattice (KL) with semimetallic conduction bands (SMCB):

$$\mathcal{H} = \sum_{\alpha=1,2}\sum_{\sigma=\uparrow,\downarrow}\int_{\boldsymbol{k}\in\mathcal{K}_\alpha} d\boldsymbol{k}\,\psi^\dagger_{\boldsymbol{k}\alpha\sigma}\xi_{\boldsymbol{k}\alpha}\psi_{\boldsymbol{k}\alpha\sigma} + \frac{1}{2}\sum_{\alpha\sigma\sigma'} J_\alpha \int d\boldsymbol{r}\,\boldsymbol{S}(\boldsymbol{r})\cdot\psi^\dagger_{\alpha\sigma}(\boldsymbol{r})\boldsymbol{\sigma}_{\sigma\sigma'}\psi_{\alpha\sigma'}(\boldsymbol{r}), \quad (1)$$

where $\psi_{\alpha\sigma}(\boldsymbol{r})$ ($\psi^\dagger_{\alpha\sigma}(\boldsymbol{r})$) is the annihilation (creation) operator of electrons at $\boldsymbol{r}$ in conduction band α with spin σ and $\xi_{\boldsymbol{k}\alpha}$ is the one-body energy of the conducting electron, $\xi_{\boldsymbol{k}\alpha} = \hbar^2(\boldsymbol{k}-\boldsymbol{K}_\alpha)^2/(2m_\alpha) - \mu_\alpha$. Note that we use the electron field operator even for the hole band ($\alpha = 2$). m_α denotes an effective mass of the conduction electrons: $m_1 > 0$ (electron) and $m_2 < 0$ (hole). The chemical potential μ_α is introduced for each bands. The condition $m_1\mu_1 = m_2\mu_2$ is satisfied in compensated metals. $\boldsymbol{K}_\alpha$ denotes the centers of electron and hole pockets, and the wave vector summation is taken over the range $|\boldsymbol{k}-\boldsymbol{K}_\alpha| < k_c$ (denoted by $\mathcal{K}_\alpha$) where k_c is a wave-vector cutoff. J_α is the Kondo coupling. The localized spin operator is given by $\boldsymbol{S}(\boldsymbol{r}) = \sum_i \boldsymbol{S}_i\delta(\boldsymbol{r}-\boldsymbol{R}_i)$ where the f-electron spins $\boldsymbol{S}_i$ are localized at the lattice sites $\boldsymbol{R}_i$. $\boldsymbol{\sigma}$ is a Pauli matrix. Schematic illustration of our model is shown in Fig. 1.

In the above, we have assumed the Kramers doublet for the f-electron degrees of freedom. On the other hand, for the non-Kramers doublet realized in f^2 configuration of U and Pr ions, which is not necessarily associated with time-reversal symmetry, the localized state is described by a pseudospin $\boldsymbol{T}$ [27,28]. This pseudospin interacts with semimetallic conduction bands through the nonmagnetic degrees of freedom $\alpha = 1, 2$. The simplest interaction takes the form

$$\mathcal{H}_{\rm int} = \frac{1}{2}\sum_{\alpha\alpha'\sigma} J\int d\boldsymbol{r}\,\boldsymbol{T}(\boldsymbol{r})\cdot\psi^\dagger_{\alpha\sigma}(\boldsymbol{r})\boldsymbol{\sigma}_{\alpha\alpha'}\psi_{\alpha'\sigma}(\boldsymbol{r}). \quad (2)$$

In this case, the equivalence between $\sigma = \uparrow$ and $\downarrow$ for conduction electrons is protected by the time-reversal symmetry and the competition arises in forming a Kondo singlet state. Since the mean-field solution is same as the Kramers case (see Appendix A), in the following we mainly focus on the Kramers system described by Eq. (1) to simplify the discussion.

Now we apply the mean-field theory which effectively describe the superconducting state resulting from the superposition of "electron" and "hole" through the multichannel Kondo effect. We first write the localized spin in terms of pseudofermion as $\boldsymbol{S}(\boldsymbol{r}) = \frac{1}{2}\sum_{\sigma\sigma'} f^\dagger_\sigma(\boldsymbol{r})\boldsymbol{\sigma}_{\sigma\sigma'}f_{\sigma'}(\boldsymbol{r})$, with the local constraint $\sum_\sigma f^\dagger_\sigma(\boldsymbol{r})f_\sigma(\boldsymbol{r}) = n_f$, where $f_\sigma(\boldsymbol{r})$ ($f^\dagger_\sigma(\boldsymbol{r})$) is the annihilation (creation) operator of the f electron and n_f is an f-electron density. This constraint is described by introducing the Lagrange's multiplier ε_f to the Hamiltonian, which plays a role of the resonant f level. The mean-fields are introduced as

$$V = \frac{3}{4}J_1\langle f_\sigma(\boldsymbol{r})\psi^\dagger_{1\sigma}(\boldsymbol{r})\rangle, \quad (3)$$

$$W = \frac{3}{4}J_2\langle f_\sigma(\boldsymbol{r})\bar{\psi}^\dagger_{2\sigma}(\boldsymbol{r})\rangle = \frac{3}{4}J_2\sum_{\sigma'}\langle f_\sigma(\boldsymbol{r})\psi_{2\sigma'}(\boldsymbol{r})\epsilon_{\sigma\sigma'}\rangle, \quad (4)$$

where $\hat{\epsilon} = i\hat{\sigma}^y$, and we have introduced the hole creation operator $\bar{\psi}^\dagger_{2\sigma}$. The mean fields V and W respectively represent "hybridization" and "pair-condensation" between the pseudofermion and the conduction electrons [17,21,29,30]. Although the mean fields V and W are introduced asymmetrically with respect to the index $\alpha = 1, 2$, this situation is related to the fact that the way of introduction of pseudofermions is not unique [29]. Hence, if we consider the physical quantities in terms of the original $\boldsymbol{S}$, the symmetries between $\alpha = 1, 2$ and between $\sigma = \uparrow, \downarrow$ are preserved. The nonzero self-consistent solution is obtained when the Kondo coupling is antiferromagnetic [see Eq. (9)]. Our pseudofermion approach is justified in the low-temperature limit where the collective Kondo effects are fully activated as in the ordinary Kondo lattice [31,32]. In this regime, the resonant f-electron level ε_f is generated near the Fermi surfaces. Hence, we take $\varepsilon_f = 0$ in the following analysis.

III. RESULTS

A. Energy dispersion

We now show the energy dispersion relation in superconducting state, which is obtained as

$$E_{\boldsymbol{k}\alpha\pm} = \frac{1}{2}\left(\xi_{\boldsymbol{k}\alpha} \pm \sqrt{\xi^2_{\boldsymbol{k}\alpha} + 4|V_\alpha|^2}\right), \quad (5)$$

for each $\boldsymbol{k} \in \mathcal{K}_\alpha$. We have defined V_α by $V_1 = V$, and $V_2 = W$. The solid lines in Fig. 2 show the dispersion relation described by Eq. (5). The single-particle spectrum has the fully opened energy gap at the Fermi level. In addition, unlike the s-wave superconductor in the Bardeen-Cooper-Schrieffer (BCS) theory, the minimal energy gap is indirect with the amplitude $E_{{\rm gap},\alpha} \sim |V_\alpha|^2/|\mu_\alpha| + |V_\alpha|^2/D_\alpha$ where D_α ($\gtrsim|\mu_\alpha|$) denotes the energy range in which the conduction electrons are involved into the condensation. This energy gap is reflected in the thermodynamic properties such as a temperature dependence of the specific heat. On the other hand, the direct energy gap shows minimum at the Fermi momentum with

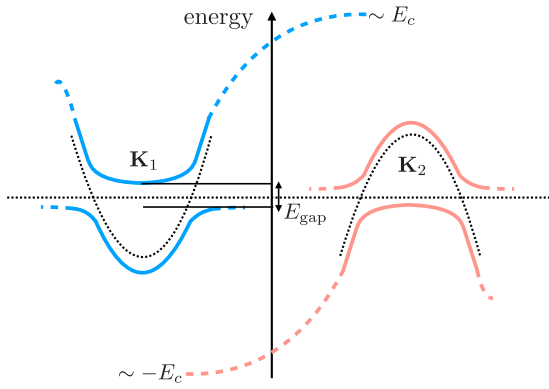

FIG. 2. Illustration for the band structures in superconducting state. The energy cutoff E_c corresponding to the band width is needed for the electromagnetic response.

its amplitude being $2|V_\alpha|$ ($\gg E_{\mathrm{gap},\alpha}$), and is reflected in the optical conductivity.[1]

B. Order parameter

Although V and W can be regarded as the order parameters in the effective model, the pseudofermions introduced to describe the low-energy excitations are not real but virtual physical degrees of freedom. Then we need to seek for the other pair amplitude that remains in the original model without considering pseudofermions. For a U(1) symmetry broken state, one naively expects a finite pair amplitude $\langle \psi_{\boldsymbol{k}\alpha\sigma}\psi_{-\boldsymbol{k},\alpha'\sigma'}\rangle$ for the conduction electrons. However, with the present effective low-energy Hamiltonian, any pair amplitude composed of conduction electrons becomes zero. This is due to the separation of the regions $\mathcal{K}_1$ and $\mathcal{K}_2$ in our model. Instead, the composite pair amplitude is the appropriate order parameter, which is given by

$$\begin{aligned}\Phi^{\alpha\alpha'}_{\mu,\sigma\sigma'}(\boldsymbol{R};\boldsymbol{r},\boldsymbol{r}') &= \langle S^\mu(\boldsymbol{R})\psi_{\alpha\sigma}(\boldsymbol{r})\psi_{\alpha'\sigma'}(\boldsymbol{r}')\rangle \\ &= \tfrac{1}{2}(\hat{\sigma}^\mu\hat{\epsilon})_{\sigma\sigma'}\epsilon_{\alpha\alpha'}V^*WF_\alpha(\boldsymbol{r}-\boldsymbol{R})F^*_{\alpha'}(\boldsymbol{r}'-\boldsymbol{R}),\end{aligned} \tag{6}$$

where the function F_α behaves as

$$F_\alpha(\boldsymbol{r}=\boldsymbol{0}) = \rho_\alpha(0)\log\left(\frac{D_\alpha|\mu_\alpha|}{|V_\alpha|^2}\right), \tag{7}$$

$$F_\alpha(|\boldsymbol{r}|\to\infty) = 2\mathrm{e}^{i\boldsymbol{K}_\alpha\cdot\boldsymbol{r}}\rho_\alpha(0)\frac{\sin(k_{\mathrm{F}\alpha}r)\mathrm{e}^{-r/\xi_\alpha}}{k_{\mathrm{F}\alpha}r}. \tag{8}$$

See Appendix B for derivation. Here, $\rho_\alpha(0)$ is the density of states of the conduction electron at the Fermi level. $k_{\mathrm{F}\alpha} = \sqrt{2m_\alpha\mu_\alpha}/\hbar$ stands for the Fermi momentum for each band. ξ_α represents the coherence length defined by $\xi_\alpha = |\mu_\alpha|/k_{\mathrm{F}\alpha}|V_\alpha|$, which is determined by the energy scale of $|V_\alpha|$. Since $E_{\mathrm{gap},\alpha} \ll |V_\alpha|$, the coherence length becomes much shorter than that expected by the amplitude of the energy gap. This is due to the nearly localized nature of the composite pairs involving the f electron.

The composite pair amplitude $\Phi(\boldsymbol{R},\boldsymbol{r},\boldsymbol{r}')$ depends on the relative coordinates $\boldsymbol{r}-\boldsymbol{R}$ and $\boldsymbol{r}'-\boldsymbol{R}$ measured from the position of the localized spin, whereas it does not depend on that between conduction electrons, $\boldsymbol{r}-\boldsymbol{r}'$. This nature reflects the superposition between the electron-Kondo singlet and the hole-Kondo singlet and not a simple pair-condensation of conduction electrons. We have thus demonstrated that the composite pair amplitude is generated in the SMCB-KL. We also comment on the relation between composite pair and odd-frequency pairing. The composite order parameter has been discussed in the context of the odd-frequency superconductor to date [12–14]. However, our result shows that, as long as the low-energy property is concerned, there is no pair amplitude between conduction electrons. In this sense, the composite order parameter does not directly mean the presence of odd-frequency pairing. This point can be clarified with our effective model in Eq. (1).

C. Self-consistent equation

The values of mean-fields can be determined by solving the self-consistent equations given as follows:

$$1 = \frac{3}{4}\frac{J_\alpha}{\Omega}\sum_{\boldsymbol{k}\in\mathcal{K}_\alpha}\frac{f(E_{\boldsymbol{k}\alpha-}) - f(E_{\boldsymbol{k}\alpha+})}{E_{\boldsymbol{k}\alpha+} - E_{\boldsymbol{k}\alpha-}}, \tag{9}$$

where $f(x) = 1/(\mathrm{e}^{\beta x}+1)$ is the Fermi-Dirac distribution function and Ω is a volume of the system. The critical temperature $T_{c,\alpha}$ can be obtained for each mean fields from the above self-consistent equation as

$$k_{\mathrm{B}}T_{c,\alpha} = \frac{2\mathrm{e}^\gamma}{\pi}\sqrt{D_\alpha|\mu_\alpha|}\exp\left[-\frac{4}{3J_\alpha\rho_\alpha(0)}\right], \tag{10}$$

where γ is the Euler constant and the prefactor is $2\mathrm{e}^\gamma/\pi \simeq 1.13$. There is also the relation $k_{\mathrm{B}}T_{c,\alpha} \propto E_{\mathrm{gap},\alpha}$, where the coefficient is order of unity but is still dependent on the parameters such as D_α and μ_α due to the magnitude relation $D_\alpha \sim |\mu_\alpha|$. See Appendix C for more details. Since only the Kondo effect is involved in our theory, the appearance of the Kondo gap is natural as the characteristic energy scale, but it is much reduced from that in the usual heavy electrons because of a small density of states in semimetals. For a rough estimation, we use the expression $T_K = D\exp(-1/\lambda)$, where D is a half bandwidth and λ is a density of states at Fermi level multiplied with the Kondo coupling. If we take the bandwidth $2D = 10^4$ K and $\lambda = 0.3$, we get $T_K \simeq 180$ K. For SMCB, λ is smaller and we get $T_K \simeq 0.2$ K when we choose $\lambda = 0.1$. We also examine the thermodynamic stability of the present ordered state in the low-temperature limit, and obtain the following free energy density $F(T) \simeq F_0(0) - 2\sum_\alpha \rho_\alpha(0)|V_\alpha|^2$, where $F_0(T)$ denotes the component in the normal state. Therefore, the composite pair amplitude contributes to the energy-lowering in the low-temperature limit. Above results are consistent with the tight-binding model calculations for the SMCB-KL. See Appendix D for details.

The energy scales of the critical temperature should be considered separately for the Kramers case and the non-Kramers case. In general, the electron and hole bands can be

[1]While we consider the completely separated electron/hole Fermi surfaces in $\boldsymbol{k}$ space, we also analyze the model with electron and hole Fermi surfaces at the same position for comparison as the opposite limit. See Appendixes D and G for more details.

asymmetric, and then $T_{c,1}$ is different from $T_{c,2}$ in the Kramers case. Since the self-consistent equations for $T_{c,1}$ and $T_{c,2}$ are independent in the low-energy effective model, the superconducting critical temperature is estimated by $T_c \sim \min(T_{c,1}, T_{c,2})$. The larger value of $T_{c,\alpha}$ is regarded as a crossover scale for the single-channel Kondo effect. For a non-Kramers doublet system, on the other hand, the equivalence of the channels is protected by the time-reversal symmetry, thus only one energy scale appears for T_c.

D. Induced pair amplitude and electromagnetic response

So far, we have considered only the degrees of freedom near the Fermi level, and concluded the presence of the composite pair amplitude in Eq. (6) and the absence of the conventional Cooper pairs. However, with this situation, the composite pairs are not carried by the external field which acts only on the conduction electrons. The Meissner effect is then absent. Hence we need to consider the secondarily induced pair amplitude among the conduction electrons for the electromagnetic response. The property of this induced pair amplitude depends on the detail of the high-energy region and is specific to the material details. As one of the origins, we consider the finite cutoff of the energy dispersion at high energy E_c ($\sim D_1, D_2$) (see Fig. 2). We note that the regions $\mathcal{K}_1$ and $\mathcal{K}_2$ now overlap with each other. Then, the induced Cooper pair is formed by an electron near the Fermi level and another one in high-energy region. This is regarded as a lattice regularization for the energy dispersion. The contribution from the high-energy region can be included perturbatively by expanding the physical quantities as a series of the orders of E_c^{-1}. (See Appendix E for derivation.) Thus the pair amplitude composed of conduction electrons can be finite in general for a tight-binding lattice, which is obtained as

$$\langle \psi_{\boldsymbol{k}\alpha\sigma}\psi_{-\boldsymbol{k},\alpha'\sigma'}\rangle = -\frac{V^*W}{E_c}\epsilon_{\sigma\sigma'}\sigma^x_{\alpha\alpha'}\sum_{\alpha''}\frac{\theta(k_c-|\boldsymbol{k}-\boldsymbol{K}_{\alpha''}|)}{\sqrt{\xi^2_{\boldsymbol{k}\alpha''}+4|V_{\alpha''}|^2}}. \tag{11}$$

The coherence length ξ_c for this induced Cooper pair is $\xi_c = \max\{\xi_1, \xi_2\}$ which is the same order of magnitude as that for the composite pairs in Eq. (6).

Electromagnetic response functions can be calculated based on the Kubo formula [33]. Within the linear response of the vector potential $\boldsymbol{A}(\boldsymbol{q})$, which is applied on the conduction electrons, we can write the total current as $j^\mu_{\rm tot} = -\sum_\nu K_{\mu\nu}A_\nu$. The introduced kernel is separated into two terms as $K_{\mu\nu} = K^d_{\mu\nu} + K^p_{\mu\nu}$, which describes diamagnetic and paramagnetic contributions, respectively. Each term is given as

$$K^p_{\mu\nu}(\boldsymbol{q}) = -\int_0^\beta d\tau\langle \hat{j}^p_\mu(\boldsymbol{q},\tau)\hat{j}^p_\nu(-\boldsymbol{q})\rangle, \tag{12}$$

$$K^d_{\mu\nu}(\boldsymbol{q}) = \delta_{\mu\nu}\frac{e^2}{\hbar^2}\sum_{\alpha,\sigma}\int\frac{d\boldsymbol{k}}{(2\pi)^3}\frac{\partial^2\varepsilon_{\boldsymbol{k}\alpha}}{\partial k^2_\mu}\langle\psi^\dagger_{\boldsymbol{k}\alpha\sigma}\psi_{\boldsymbol{k}\alpha\sigma}\rangle. \tag{13}$$

The paramagnetic current operator $\hat{j}^p_\mu$ is defined as

$$\hat{\boldsymbol{j}}^p(\boldsymbol{q}) = e\sum_{\alpha,\sigma}\int d\boldsymbol{k}\,\psi^\dagger_{\boldsymbol{k}-\boldsymbol{q}/2,\alpha\sigma}\boldsymbol{v}_{\boldsymbol{k}\alpha}\psi_{\boldsymbol{k}+\boldsymbol{q}/2,\alpha\sigma}, \tag{14}$$

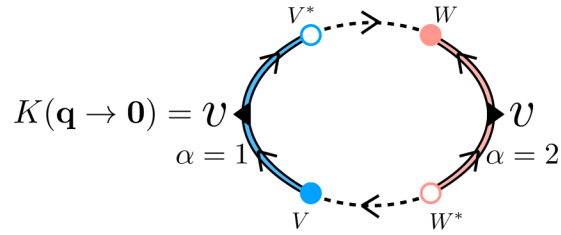

FIG. 3. Illustration for the lowest-order diagram that contributes to the Meissner kernel. The blue (pink) solid and the black dashed lines with the arrow represent the conduction electron in the electron (hole) band and the pseudofermion, respectively.

where $e < 0$ denotes the charge of the electron and $\boldsymbol{v}_{\boldsymbol{k}\alpha} = \hbar^{-1}\partial_{\boldsymbol{k}}\varepsilon_{\boldsymbol{k}\alpha}$ is the velocity. We note that the energy $\varepsilon_{\boldsymbol{k}\alpha}$ represents the tight-binding band and includes the high-energy part shown in Fig. 2.

We neglect the vertex correction for the current correlation function as in the dynamical mean-field theory which is exact in infinite dimensions and is regarded as a good approximation for three dimensions [34,35]. Then the leading-order contribution to the response function is diagramatically shown in Fig. 3. At zero temperature, the electromagnetic kernel is evaluated as

$$K_{\mu\nu}(\boldsymbol{q}\to\boldsymbol{0}) \simeq \sum_\alpha\frac{4|V_1|^2|V_2|^2}{|V_\alpha|^2E_c^2}\frac{n_\alpha e^2}{|\tilde{m}_\alpha|}\delta_{\mu\nu}, \tag{15}$$

where n_α is the particle number of the electron ($\alpha = 1$) and the hole ($\alpha = 2$). We note that n_2 is written by hole operators as $n_2 = \sum_\sigma\langle\bar{\psi}^\dagger_{2\sigma}\bar{\psi}_{2\sigma}\rangle$. $\tilde{m}_\alpha(\sim -m_\alpha)$ denotes the effective mass of $\varepsilon_{\boldsymbol{k}\bar{\alpha}}$ with $\boldsymbol{k}\in\mathcal{K}_\alpha$ (here $\bar{\alpha}$ is the complementary component of α such as $\bar{1} = 2$). See Appendix F for the detailed derivation. The magnitude of the kernel is smaller than the usual BCS superconductors by the factor of $(|V_\alpha|/E_c)^2$. Hence, the superconducting state has a large magnetic penetration depth reflecting the small Cooper pair amplitude $\langle\psi_{\boldsymbol{k}\alpha\sigma}\psi_{-\boldsymbol{k},\alpha'\sigma'}\rangle$. This is because both K^p and K^d have the finite and almost the same amplitudes at zero temperature. Therefore the cancellation between them occurs, and the situation is similar to that for the normal Kondo insulator. In the presence of the induced pair amplitude, however, the paramagnetic (diamagnetic) term slightly decreases (increases). The remaining contribution, which is the order of E_c^{-2}, plays a role of the superconducting current (See Appendix F). In this way, although the induced pair amplitude does not contribute to the condensation energy as we mentioned in the previous section, it plays an essential role for the electromagnetic response expected in the superconducting state.

IV. DISCUSSION

We here comment on the consideration of some competing orders. In the correlated semimetals, excitonic insulator states [9–11] or metallic CDWs [36] would compete with the present mechanism of superconductivity. While such instabilities arise only when the conduction bands have a nesting of the Fermi surface, the present mechanism works when there are the semimetallic conduction bands regardless of the details of Fermi surfaces.

Finally, let us discuss the candidate materials of the present superconducting state. We propose the two relevant materials UBe_{13} [5] and $PrIr_2Zn_{20}$ [37]. For UBe_{13}, the system undergoes a phase transition into unconventional superconductivity from a non-Fermi liquid state, and the multichannel Kondo effect has been suspected as a cause [27,28]. We speculate that UBe_{13} can be a candidate material for our scenario based on the following two reasonable assumptions. First, as seen from its chemical composition, the number of Be inside the unit-cell is much larger than the magnetic uranium ion. Therefore the presence of the uranium atom does not affect much the conduction band structure. Second, the electronic structure of Be in the atomic limit is partially filled L shell, which is composed of fully filled $2s$ orbital and empty $2p$ orbital. In a crystal environment, the s band and the p band resulting from the interberylium hopping bury the atomic gap and the semimetallic conduction bands are formed. Indeed, the electronic structures of the elemental substance of Be has a semimetallic character [38,39]. Hence, UBe_{13} can be regarded as the embedded magnetic U atom in the sea of the electrons which have electron and hole conduction bands. Thus the SMCB-KL considered in this paper can be realized in this material.

As for Pr-based materials, $PrIr_2Zn_{20}$, shows a peculiar superconductivity with the multi-channel Kondo behavior [37,40], can also be regarded as the promising candidate material for the SMCB-KL, since the Zn has the fully filled $3d$ and $4s$ orbitals and an energy gap is needed to locate an additional electron in higher-energy $4p$ orbital. Indeed the elemental substance of Zn shows semimetallic character [41,42]. In addition, the number of Zn is much larger than that of Pr. Hence the situation is close to UBe_{13}, and the formation of the SMCB-KL is expected. Further studies such as realistic band calculations combined with electronic correlation effects are needed to establish the actual realization of our proposal in real materials, which are left as interesting future issues.

V. SUMMARY

Based on the mean-field theory, we have established the mechanism for the full-gap superconductivity characteristic for the semimetals along with the localized spin/pseudospins and have elucidated the physical properties of the superconducting state. The energy dispersion has the full-gap nature, where the minimum gap is indirect unlike the s-wave BCS superconductor. Its characteristic energy scale is given by the Kondo gap, where the magnitude is much reduced from that in the usual heavy-electron material because of the small density of states at the Fermi level in semimetals. We have roughly estimated the energy scale of the critical temperature, which is consistent to that in the heavy-electron superconductors.

Focusing on the low-energy region, we have shown that the primary order parameter is the composite pair amplitude, which describes the three-body bound states of the conduction electron, hole and the localized spin moment. We have elucidated the spatial correlation of the composite pair amplitude, which depends on the relative coordinates of the conduction electron and hole measured from the localized spin moment, whereas it does not depend on the distance between the conduction electrons. Hence, the formation of the composite pair amplitude can be interpreted as the superposition between the electron Kondo-singlet and the hole Kondo singlet. In addition, we have clarified the mechanism of the Meissner effect, where the system responds to the electromagnetic potential through the formation of the secondarily induced Cooper pair among an electron near the Fermi level and the another one in high-energy region.

We have also discussed the possible realization in the realistic materials UBe_{13} and $PrIr_2Zn_{20}$ based on the characteristic chemical composition of these materials. In addition to these compounds, the idea of the SMCB-KL can be applied to a wider class of materials with the semimetallic conduction bands plus localized moments, and gives a general guiding principle to find unconventional superconductors.

ACKNOWLEDGMENTS

This work was supported by the Japan Society for Promotion of Science (JSPS) KAKENHI Grants No. 16H04021, No. 18H01176, and No. 18H04305.

APPENDIX A: MEAN-FIELD APPROXIMATION

In this section, we employ the mean-field approximation and decouple the interaction between conduction electrons and Kramers/non-Kramers doublet. Hereafter, we take $\hbar$ as unity.

1. Kramers doublet system

For the Kramers doublet, the interaction term is described by the pseudofermion operator $f_\sigma(\boldsymbol{r})$ as follows:

$$\mathcal{H}_{\rm int} = \frac{1}{4}\sum_{\sigma_1\sigma_2}\sum_{\alpha,\sigma\sigma'} J_\alpha \int d\boldsymbol{r} \times f^\dagger_{\sigma_1}(\boldsymbol{r})\boldsymbol{\sigma}_{\sigma_1\sigma_2} f_{\sigma_2}(\boldsymbol{r}) \cdot \psi^\dagger_{\alpha\sigma}(\boldsymbol{r})\boldsymbol{\sigma}_{\sigma\sigma'}\psi_{\alpha\sigma'}(\boldsymbol{r}). \tag{A1}$$

The interaction between the electron Fermi surface and the localized spin is decoupled as

$$\mathcal{H}_{{\rm int},\alpha=1} \simeq \sum_\sigma \int d\boldsymbol{k}\, V^* \psi^\dagger_{\boldsymbol{k}1\sigma} f_{\boldsymbol{k}\sigma} + {\rm H.c.}, \tag{A2}$$

where V represents the mean-field defined in Eq. (3). Similarly, we decouple the interaction between the hole surface and the localized spin as

$$\mathcal{H}_{{\rm int},\alpha=2} \simeq \sum_\sigma \int d\boldsymbol{k}\, W^* \epsilon_{\sigma\bar\sigma} \psi_{-\boldsymbol{k}2\bar\sigma} f_{\boldsymbol{k}\sigma} + {\rm H.c.}, \tag{A3}$$

where W is defined in Eq. (4). Hence, the mean-field Hamiltonian for the Kramers doublet is given by

$$\mathcal{H}^{\rm MF} = \sum_\sigma \int d\boldsymbol{k}\, \Psi^\dagger_{\boldsymbol{k}\sigma} \begin{pmatrix} \xi_{\boldsymbol{k}1} & 0 & V^* \\ 0 & -\xi_{\boldsymbol{k}2} & W^*\epsilon_{\sigma\bar\sigma} \\ V & W\epsilon_{\sigma\bar\sigma} & 0 \end{pmatrix} \Psi_{\boldsymbol{k}\sigma}, \tag{A4}$$

where the Nambu representation of the field operators is defined as follows:

$$\Psi^{\dagger}_{\boldsymbol{k}\sigma} = (\psi^{\dagger}_{\boldsymbol{k}1\sigma}, \psi_{-\boldsymbol{k}2\bar{\sigma}}, f^{\dagger}_{\boldsymbol{k}\sigma}). \tag{A5}$$

2. Non-Kramers doublet system

We introduce the pseudofermion operator $d_\alpha(\boldsymbol{r})$, which describes the pseudospin degrees of freedom. The localized pseudospin operator $\boldsymbol{T}(\boldsymbol{r})$ can be rewritten in terms of the pseudofermion as $\boldsymbol{T}(\boldsymbol{r}) = \frac{1}{2}\sum_{\alpha\alpha'} d^{\dagger}_{\alpha}(\boldsymbol{r})\boldsymbol{\sigma}_{\alpha\alpha'}d_{\alpha'}(\boldsymbol{r})$ with the local constraint $\sum_\alpha d^{\dagger}_{\alpha}(\boldsymbol{r})d_\alpha(\boldsymbol{r}) = n_f$. Then, the interaction between the non-Kramers doublet and the semimetallic conduction bands is described as follows:

$$\mathcal{H}_{\rm int} = \frac{1}{4}\sum_{\alpha_1\alpha_2}\sum_{\alpha\alpha',\sigma} J\int d\boldsymbol{r} \times d^{\dagger}_{\alpha_1}(\boldsymbol{r})\boldsymbol{\sigma}_{\alpha_1\alpha_2}d_{\alpha_2}(\boldsymbol{r})\cdot\psi^{\dagger}_{\alpha\sigma}(\boldsymbol{r})\boldsymbol{\sigma}_{\alpha\alpha'}\psi_{\alpha'\sigma}(\boldsymbol{r}). \tag{A6}$$

We introduce the following mean fields:

$$\tilde{V}_\alpha = \tfrac{3}{4}J\langle d_\alpha(\boldsymbol{r})\psi^{\dagger}_{\alpha\uparrow}(\boldsymbol{r})\rangle, \tag{A7}$$

$$\tilde{W}_{\alpha'}\epsilon_{\alpha\alpha'} = \tfrac{3}{4}J\langle d_\alpha(\boldsymbol{r})\psi_{\alpha'\downarrow}(\boldsymbol{r})\rangle. \tag{A8}$$

The resultant mean-field Hamiltonian is given by

$$\mathcal{H}^{\rm MF} = \sum_\alpha\int d\boldsymbol{k}\,\tilde{\Psi}^{\dagger}_{\boldsymbol{k}\alpha}\begin{pmatrix}\xi_{\boldsymbol{k}\alpha} & 0 & \tilde{V}^{*}_{\alpha}\\ 0 & -\xi_{\boldsymbol{k}\bar{\alpha}} & \tilde{W}^{*}_{\bar{\alpha}}\epsilon_{\alpha\bar{\alpha}}\\ \tilde{V}_\alpha & \tilde{W}_{\bar{\alpha}}\epsilon_{\alpha\bar{\alpha}} & 0\end{pmatrix}\tilde{\Psi}_{\boldsymbol{k}\alpha}, \tag{A9}$$

where $\tilde{\Psi}^{\dagger}_{\boldsymbol{k}\alpha} = (\psi^{\dagger}_{\boldsymbol{k}\alpha\uparrow} \quad \psi_{-\boldsymbol{k}\bar{\alpha}\downarrow} \quad d^{\dagger}_{\boldsymbol{k}\alpha})$.

3. Validity of mean-field theory

We comment on the validity of our mean-field approach to the Kondo lattice with semimetallic conduction bands. For a typical heavy-electron system, the localized moments of f electrons at high temperatures crossover to the heavy-electron state at low temperatures by a collective Kondo effect. It is recognized that the mean-field approximation, which we have used in our paper, changes the crossover into the transition, which is an artifact of the approximation. On the other hand, the ground state with heavy electrons is correctly reproduced by the mean-field theory, and the transition temperature predicts the crossover energy scale obtained in the more accurate method. For example, the comparison has been done in the study of two-dimensional Kondo lattice [32].

The justification for the use of the mean-field theory has been demonstrated also in the two-channel Kondo lattice models. The dynamical mean-field theory, which takes full account of local electronic correlation necessary for the Kondo effects, has revealed several nontrivial ordered phases including unconventional superconductivity [24,43]. These results are reasonably reproduced by the mean-field theory as demonstrated in Ref. [29]. In the present work, we apply this established method to the Kondo lattice problem with semimetallic conduction bands.

APPENDIX B: COMPOSITE ORDER PARAMETER AND CORRELATION

In this section, we evaluate the composite pair amplitude, which is defined in Eq. (6). It can be rewritten in the mean-field theory as follows:

$$\Phi^{\alpha\alpha'}_{\mu,\sigma\sigma'}(\boldsymbol{R};\boldsymbol{r},\boldsymbol{r}') \simeq \frac{1}{2}\sum_{\sigma_1,\sigma_2}\sigma^{\mu}_{\sigma_1\sigma_2}[\delta_{\alpha1}\delta_{\alpha'2}\delta_{\sigma_1\sigma}F_{1\sigma}(\boldsymbol{r}-\boldsymbol{R})F_{2\sigma_2\sigma'}(\boldsymbol{r}'-\boldsymbol{R}) - \delta_{\alpha2}\delta_{\alpha'1}\delta_{\sigma_1\sigma'}F_{1\sigma'}(\boldsymbol{r}'-\boldsymbol{R})F_{2\sigma_2\sigma}(\boldsymbol{r}-\boldsymbol{R})], \tag{B1}$$

where $F_{1\sigma}(\boldsymbol{r})$ and $F_{2\sigma\sigma'}(\boldsymbol{r})$ are defined respectively as

$$F_{1\sigma}(\boldsymbol{r}) \equiv \frac{1}{\Omega}\sum_{\boldsymbol{k}}\langle\psi_{\boldsymbol{k}1\sigma}f^{\dagger}_{\boldsymbol{k}\sigma}\rangle e^{i\boldsymbol{k}\cdot\boldsymbol{r}}, \tag{B2}$$

$$F_{2\sigma\sigma'}(\boldsymbol{r}) \equiv \frac{1}{\Omega}\sum_{\boldsymbol{k}}\langle f_{\boldsymbol{k}\sigma}\psi_{-\boldsymbol{k}2\sigma'}\rangle e^{-i\boldsymbol{k}\cdot\boldsymbol{r}}. \tag{B3}$$

In the low-temperature limit, $F_{1\sigma}(\boldsymbol{r})$ and $F_{2\sigma\sigma'}(\boldsymbol{r})$ can be rewritten as follows:

$$F_{1\sigma}(\boldsymbol{r}) = \frac{V^*}{\Omega}\sum_{\boldsymbol{k}\in\mathcal{K}_1}\frac{f(E_{\boldsymbol{k}1-})-f(E_{\boldsymbol{k}1+})}{E_{\boldsymbol{k}1+}-E_{\boldsymbol{k}1-}}e^{i\boldsymbol{k}\cdot\boldsymbol{r}} = \frac{V^*}{(2\pi)^3}\int_{\boldsymbol{k}\in\mathcal{K}_1}d\boldsymbol{k}\frac{e^{i\boldsymbol{k}\cdot\boldsymbol{r}}}{\sqrt{\xi^2_{\boldsymbol{k}1}+4|V|^2}} \equiv V^*F_1(\boldsymbol{r}), \tag{B4}$$

$$F_{2\sigma\sigma'}(\boldsymbol{r}) = \frac{W\epsilon_{\sigma\sigma'}}{\Omega}\sum_{\boldsymbol{k}\in\mathcal{K}_2}\frac{f(E_{\boldsymbol{k}2-})-f(E_{\boldsymbol{k}2+})}{E_{\boldsymbol{k}2+}-E_{\boldsymbol{k}2-}}e^{-i\boldsymbol{k}\cdot\boldsymbol{r}} = \frac{W\epsilon_{\sigma\sigma'}}{(2\pi)^3}\int_{\boldsymbol{k}\in\mathcal{K}_2}d\boldsymbol{k}\frac{e^{-i\boldsymbol{k}\cdot\boldsymbol{r}}}{\sqrt{\xi^2_{\boldsymbol{k}2}+4|W|^2}} \equiv W\epsilon_{\sigma\sigma'}F^*_2(\boldsymbol{r}). \tag{B5}$$

Therefore, we obtain the composite pair amplitude given in Eq. (6).

We derive the behavior of $F_\alpha(\boldsymbol{r})$ given in Eqs. (7) and (8) below. First, we integrate the angular valuables since the energy dispersion is isotropic around $\boldsymbol{K}_\alpha$. Then, $F_\alpha(\boldsymbol{r})$ is rewritten as follows:

$$F_\alpha(\boldsymbol{r}) = \frac{e^{i\boldsymbol{K}_\alpha\cdot\boldsymbol{r}}}{k_{\rm F\alpha}r}s_\alpha\int_{-\mu_\alpha}^{s_\alpha D_\alpha}d\epsilon\,\rho_\alpha(\epsilon)\frac{\sin\left(k_{\rm F\alpha}r\sqrt{1+\frac{\epsilon}{\mu_\alpha}}\right)}{\sqrt{\left(1+\frac{\epsilon}{\mu_\alpha}\right)(\epsilon^2+4|V_\alpha|^2)}}, \tag{B6}$$

where $s_\alpha = \sigma^z_{\alpha\alpha}$. $\rho_\alpha(\epsilon) = \sum_{\boldsymbol{k}}\delta(\epsilon-\xi_{\boldsymbol{k}\alpha})/\Omega$ represents the density of states (DOS) of the bare conduction electrons. Hereafter, we use the constant DOS for $\rho_\alpha(\epsilon)$ to simplify the following calculations.

At $\boldsymbol{r}=\boldsymbol{0}$, $F_\alpha(\boldsymbol{0})$ is rewritten as

$$F_\alpha(\boldsymbol{0}) = s_\alpha\int_{-\mu_\alpha}^{s_\alpha D_\alpha}d\epsilon\,\rho_\alpha(\epsilon)\frac{1}{\sqrt{\epsilon^2+4|V_\alpha|^2}} \simeq \rho_\alpha(0)\log\left(\frac{D_\alpha|\mu_\alpha|}{|V_\alpha|^2}\right). \tag{B7}$$

On the other hand, we can obtain the following representation for $|\boldsymbol{r}| \to \infty$:

$$F_\alpha(|\boldsymbol{r}| \to \infty) \simeq 2e^{i\boldsymbol{K}_\alpha\cdot\boldsymbol{r}}\rho_\alpha(0)\frac{\sin(k_{F\alpha}r)}{k_{F\alpha}r}K_0\left(\frac{r}{\xi_\alpha}\right), \tag{B8}$$

where we have used $|V_\alpha| \ll D_\alpha, |\mu_\alpha|$. $K_0(z)$ is a zeroth-modified Bessel function of the second kind, and is given by $K_0(z) = \int_0^\infty dx \cos(zx)/\sqrt{1+x^2}$. Since $K_0(z)$ behaves as $K_0(z) \sim e^{-z}$ for $|z| \gg 1$, $F_\alpha(\boldsymbol{r})$ for $r \gg \xi_\alpha$ is given as Eq. (8).

APPENDIX C: SELF-CONSISTENT EQUATIONS FOR MEAN FIELDS

In this section, we derive the self-consistent equation for the effective mean fields V and W. Equations (3) and (4) can be rewritten by utilizing the calculations in Eqs. (B4) and (B5), as

$$1 = \frac{3}{4}\frac{J_\alpha}{\Omega}\sum_{\boldsymbol{k}}\frac{f(E_{\boldsymbol{k}\alpha-}) - f(E_{\boldsymbol{k}\alpha+})}{E_{\boldsymbol{k}\alpha+} - E_{\boldsymbol{k}\alpha-}}. \tag{C1}$$

Now, we derive the critical temperature $T_{c,\alpha}$ for the mean-field V_α.

At the critical temperature, the amplitude of the mean-field becomes 0, and the self-consistent equation is rewritten as follows:

$$1 \simeq \frac{3}{8}J_\alpha\rho_\alpha(0)\int_{-|\mu_\alpha|}^{D_\alpha} d\epsilon \frac{\tanh\left(\frac{|\epsilon|}{2k_BT_c}\right)}{|\epsilon|}. \tag{C2}$$

The integration is similar to that appears in the BCS theory. Thus we can obtain the critical temperature in Eq. (10).

On the other hand, since the self-consistent equation is rewritten as $1 \simeq (3J_\alpha/4)F_\alpha(\boldsymbol{0})$ at zero temperature, we obtain the amplitude of the mean field as

$$|V_\alpha(T=0)| \simeq \sqrt{D_\alpha|\mu_\alpha|}\exp\left[-\frac{2}{3J_\alpha\rho_\alpha(0)}\right]. \tag{C3}$$

From above, the ratio between $T_{c,\alpha}$ and the amplitude of the energy gap $E_{\mathrm{gap},\alpha} = |V_\alpha|^2/|\mu_\alpha| + |V_\alpha|^2/D_\alpha$ at zero temperature is given by

$$\frac{E_{\mathrm{gap},\alpha}}{k_BT_{c,\alpha}} = \frac{\pi}{2e^\gamma} \times \frac{D_\alpha + |\mu_\alpha|}{\sqrt{D_\alpha|\mu_\alpha|}}. \tag{C4}$$

In the above calculations, we have used the constant DOS for simplicity. Once the energy dependence of the DOS is considered, the constant in Eq. (10) is modified from 1.13. This is due to the fact that the Fermi energy μ_α and energy range D_α have same orders of magnitude. In contrast, for BCS superconductors, the energy scales of Fermi energy and Debye frequency are much separated, so the prefactor in the expression of T_c is universal.

APPENDIX D: NUMERICAL CALCULATIONS BY TIGHT-BINDING MODEL

In this section, in order to further support our results obtained by the low-energy effective theory focused on the degrees of freedom near the Fermi level, we perform the numerical calculation in two-dimensional square lattice. The

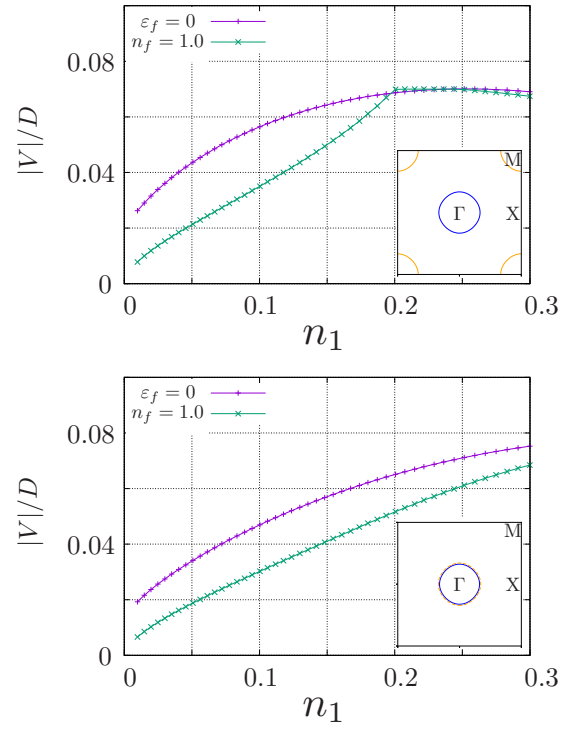

FIG. 4. Order parameter $|V| = |W|$ is plotted as a function of n_1, which is the original number of conduction electrons in electron Fermi surface. The Kondo coupling is $J_1/D = J_2/D = 0.4$, where $D = 8t$ is the band width. Temperature is $T = 2.5 \times 10^{-4}D$. The number of $\boldsymbol{k}$ mesh is 300^2.

tight-binding model for the Kramers doublet system is given by

$$\mathcal{H} = \sum_{\alpha=1,2}\sum_{\boldsymbol{k}\sigma}\xi_{\boldsymbol{k}\alpha}c^\dagger_{\boldsymbol{k}\alpha\sigma}c_{\boldsymbol{k}\alpha\sigma} + \frac{1}{2}\sum_i\sum_{\alpha=1,2}\sum_{\sigma,\sigma'}J_\alpha\boldsymbol{S}_i\cdot c^\dagger_{i\alpha\sigma}\boldsymbol{\sigma}_{\sigma\sigma'}c_{i\alpha\sigma'}, \tag{D1}$$

where $c_{i\alpha\sigma}(c^\dagger_{i\alpha\sigma})$ denotes the annihilation operator of the conduction electron at site i. $\boldsymbol{S}_i$ represents the localized spin moment. The non-Kramers doublet case is separately considered, which will be discussed at the end of this section. The energy dispersion $\xi_{\boldsymbol{k}\alpha}$ is given by

$$\xi_{\boldsymbol{k}\alpha} = -2t(\cos k_x + \cos k_y) - \sigma^z_{\alpha\alpha}\mu, \tag{D2}$$

where the lattice constant is taken as unity and $k_{x,y} \in [-\pi, \pi)$. t denotes the hopping amplitude between the nearest neighbor sites. The potential μ pushes up the $\alpha = 1$ band to form an electron Fermi surface, and pushes down the $\alpha = 2$ band to form a hole Fermi surface (see insets of Fig. 4).

We introduce the pseudofermion representation of the localized spin $\boldsymbol{S}_i = \frac{1}{2}\sum_{\sigma\sigma'}f^\dagger_{i\sigma}\boldsymbol{\sigma}_{\sigma\sigma'}f_{i\sigma'}$. In order to describe the constraint on the number of the pseudofermion $\sum_\sigma\langle f^\dagger_{i\sigma}f_{i\sigma}\rangle = n_f$, we introduce the Lagrange's multiplier ε_f, which plays a role of the resonant f-level in the coherent Kondo effect. Since the presence of the Fermi surfaces in conduction bands is responsible for the Kondo effect, it is natural to consider that the resonant f level is formed at the Fermi level. Hence

we choose $\varepsilon_f = 0$ as in the main text and only the degrees of freedom near the Fermi level matter. On the other hand, if one assumes that all the localized spins at every site provide the fermionic degrees of freedom, the constraint $n_f = 1$ is used. Below we show the results for both cases.

The mean-field amplitudes are given by

$$V = \tfrac{3}{4}J_1\langle f_{i\sigma}c^\dagger_{i1\sigma}\rangle, \tag{D3}$$

$$W\epsilon_{\sigma\bar{\sigma}} = \tfrac{3}{4}J_2\langle f_{i\sigma}c_{i2\bar{\sigma}}\rangle. \tag{D4}$$

The resultant mean-field Hamiltonian is obtained as follows:

$$\mathcal{H}^{\rm MF} = \sum_{\boldsymbol{k},\sigma}\Psi^\dagger_{\boldsymbol{k}\sigma}\begin{pmatrix}\xi_{\boldsymbol{k}1} & 0 & V^* \\ 0 & -\xi_{\boldsymbol{k}2} & W^*\epsilon_{\sigma\bar{\sigma}} \\ V & W\epsilon_{\sigma\bar{\sigma}} & \varepsilon_f\end{pmatrix}\Psi_{\boldsymbol{k}\sigma}, \tag{D5}$$

where $\Psi^\dagger_{\boldsymbol{k}\sigma} = (c^\dagger_{\boldsymbol{k}1\sigma} \quad c_{-\boldsymbol{k}2\bar{\sigma}} \quad f^\dagger_{\boldsymbol{k}\sigma})$. We have solved the self-consistent equations obtained from Eqs. (D3) and (D4) by iterative method. Figure 4 shows the mean-field solution of the order parameter as a function of the electron number (n_1) of $\alpha = 1$ (electron band) in the normal state. Upper panel shows the result for semimetal systems, where electron and hole Fermi surfaces are separated in the momentum space. Schematic pictures for Fermi surfaces are shown in the inset. For all parameters shown in Fig. 4, $|V| = |W|$ is satisfied, and hence the superconductivity is realized. Purple lines represent the results for $\varepsilon_f = 0$, where the superconducting state has always the full-gap nature. Green lines denote the results for $n_f = 1$. In $0.2 \lesssim n_1 \lesssim 0.25$ in upper panel, the full-gap superconducting state is realized, while the carrier is doped in the other regions. The reason for the carrier doping is that the particle-hole symmetry is broken since the pseudofermion $f_{\uparrow,\downarrow}$ hybridizes with the conduction bands $(\xi_{\boldsymbol{k}1}, -\xi_{\boldsymbol{k}2})$ [see Eq. (A4)] to form the heavy-electron band as shown in Fig. 2.

On the other hand, in the non-Kramers doublet systems, the pseudofermions d_1 and d_2 are introduced from the pseudospin operator $\boldsymbol{T}$. In this case, the form of the mean-field equations is same as that in the Kramers doublet case if we look at the one of the block-diagonal parts in the Hamiltonian. However, the constraint $\langle d^\dagger_1 d_1 + d^\dagger_2 d_2\rangle = 1$ is here satisfied together with $\varepsilon_f = 0$ in strong contrast with the Kramers doublet case. This is because the pseudofermions d_1 and d_2 respectively hybridize with the conduction bands $(\xi_{\boldsymbol{k}1}, -\xi_{\boldsymbol{k}2})$ and $(-\xi_{\boldsymbol{k}1}, \xi_{\boldsymbol{k}2})$ [see also Eq. (A9)], where the particle-hole symmetry is still preserved. Hence, the full-gap superconducting phase is robustly realized in the non-Kramers doublet case.

For reference, we also perform the calculation for the case where electron and hole surfaces are located at the same position, which is obtained by shifting $k_{x,y}$ by π for $\alpha = 2$ in Eq. (D2) (see also Appendix G). The results are shown in lower panel of Fig. 4. The superconducting gap is always closed to form the Bogoliubov-Fermi surface [44] for all parameter regions in the lower panel (unseparated case). (See Appendix G for more details.)

APPENDIX E: INDUCED PAIR AMPLITUDE

Now, we consider the band cutoff at the high-energy E_c, which is regarded as a lattice regularization. Schematic illustration for the band cutoff is shown in Fig. 5. If E_c is finite, the anomalous part of the electron Green's function $\tilde{\mathcal{F}}^{\alpha\alpha'}_{\boldsymbol{k},\sigma\sigma'}(i\omega_n) = \int_0^\beta d\tau\langle -T_\tau[\psi_{\boldsymbol{k}\alpha\sigma}(\tau)\psi_{-\boldsymbol{k}\alpha'\sigma'}]\rangle e^{i\omega_n\tau}$, where $\omega_n = (2n+1)\pi/\beta$ is fermionic Matsubara frequency is given as follows:

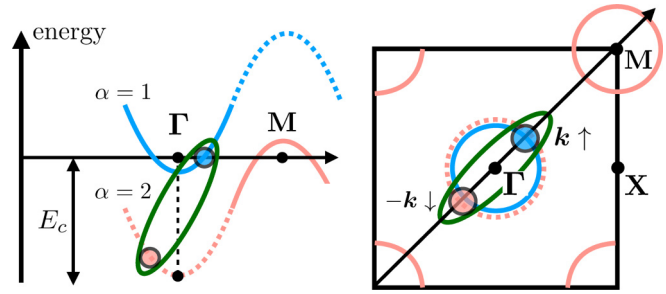

FIG. 5. Schematic pictures of the band cutoff and the induced pair amplitude. Left panel shows the energy dispersion including the finite band cutoff E_c. Right panel shows the semimetallic Fermi surfaces (solid lines) and the high-energy counterpart (dashed line), which is involved in the Cooper pair formation schematically. We used the Brillouin zone in the square lattice for a simplicity. Green ellipse drawn by solid line represents the Cooper pair formation between conduction electron near the Fermi level and another in the high-energy region.

$$\tilde{\mathcal{F}}^{\alpha\alpha'}_{\boldsymbol{k},\sigma\sigma'}(i\omega_n) = \epsilon_{\alpha\alpha'}\epsilon_{\sigma\sigma'}\frac{s_\alpha V^* W}{\bar{D}_{\boldsymbol{k}}(s_\alpha i\omega_n)}, \tag{E1}$$

where $\bar{D}_{\boldsymbol{k}}(z)$ is a function of a complex number z. It is defined as $\bar{D}_{\boldsymbol{k}}(z) = zy_{\boldsymbol{k}1}y_{\boldsymbol{k}2} - |V|^2 y_{\boldsymbol{k}2} - |W|^2 y_{\boldsymbol{k}1}$, where $y_{\boldsymbol{k}\alpha} = z - s_\alpha\xi_{\boldsymbol{k}\alpha}$. When $\boldsymbol{k} \in \mathcal{K}_\alpha$, $|\xi_{\boldsymbol{k}\bar{\alpha}}|$ is replaced with E_c ($\gg |\xi_{\boldsymbol{k}\alpha}|, |V|, |W|$), and $\tilde{\mathcal{F}}^{\alpha\alpha'}_{\boldsymbol{k},\sigma\sigma'}(i\omega_n)$ is rewritten as follows:

$$\tilde{\mathcal{F}}^{\alpha\alpha'}_{\boldsymbol{k},\sigma\sigma'}(i\omega_n) \simeq -\epsilon_{\sigma\sigma'}\frac{V^*W}{E_c}\left[\sigma^x_{\alpha\alpha'}F^e_{\boldsymbol{k}}(i\omega_n) + \epsilon_{\alpha\alpha'}F^o_{\boldsymbol{k}}(i\omega_n)\right], \tag{E2}$$

with

$$F^e_{\boldsymbol{k}}(i\omega_n) = \frac{1}{2}\sum_{\Lambda=\pm1}\sum_\alpha\frac{\theta(k_c - |\boldsymbol{k} - \boldsymbol{K}_\alpha|)}{(i\omega_n - \Lambda s_\alpha E_{\boldsymbol{k}\alpha+})(i\omega_n - \Lambda s_\alpha E_{\boldsymbol{k}\alpha-})}, \tag{E3}$$

$$F^o_{\boldsymbol{k}}(i\omega_n) = \frac{1}{2}\sum_{\Lambda=\pm1}\sum_\alpha\frac{\Lambda\theta(k_c - |\boldsymbol{k} - \boldsymbol{K}_\alpha|)}{(i\omega_n - \Lambda s_\alpha E_{\boldsymbol{k}\alpha+})(i\omega_n - \Lambda s_\alpha E_{\boldsymbol{k}\alpha-})}, \tag{E4}$$

where $F^e_{\boldsymbol{k}}(i\omega_n)$ and $F^o_{\boldsymbol{k}}(i\omega_n)$ are even and odd with respect to the Matsubara frequency, respectively.

To elucidate the relation between the secondarily induced Cooper pair amplitude and the primary order parameter, we here consider the equation of motion of the Cooper pair amplitude, which is given by

$$(-\partial_\tau - \xi_{\boldsymbol{k}\alpha})\tilde{\mathcal{F}}^{\alpha\alpha'}_{\boldsymbol{k},\sigma\sigma'}(\tau) = -\frac{J_\alpha}{2}\sum_{\sigma''}\int\frac{d\boldsymbol{q}}{(2\pi)^3}\sigma^\mu_{\sigma\sigma''}\Phi^{\alpha\alpha'}_{\mu,\sigma''\sigma'}(\tau;\boldsymbol{k}+\boldsymbol{q}\tau,-\boldsymbol{k}0), \tag{E5}$$

where $\Phi^{\alpha\alpha'}_{\mu,\sigma\sigma'}(\tau;\boldsymbol{k}_1\tau_1,\boldsymbol{k}_2\tau_2)$ is the Fourier component of the composite order parameter, which is defined as

$$\Phi^{\alpha\alpha'}_{\mu,\sigma\sigma'}(\tau;\boldsymbol{k}_1\tau_1,\boldsymbol{k}_2\tau_2) = \int d\boldsymbol{r}\int d\boldsymbol{r}' e^{-i\boldsymbol{k}_1\cdot\boldsymbol{r}} e^{-i\boldsymbol{k}_2\cdot\boldsymbol{r}'}\Phi^{\alpha\alpha'}_{\mu,\sigma\sigma'}(\boldsymbol{0}\tau;\boldsymbol{r}\tau_1,\boldsymbol{r}'\tau_2). \quad \text{(E6)}$$

We here introduced the imaginary-time representation of the composite pair amplitude as $\Phi^{\alpha\alpha'}_{\mu,\sigma\sigma'}(\boldsymbol{R}\tau;\boldsymbol{r}\tau_1,\boldsymbol{r}'\tau_2) = \langle T_\tau[S^\mu(\boldsymbol{R},\tau)\psi_{\alpha\sigma}(\boldsymbol{r},\tau_1)\psi_{\alpha'\sigma'}(\boldsymbol{r}',\tau_2)]\rangle$. Hence, the Cooper pair amplitude is rewritten as follows:

$$\tilde{\mathcal{F}}^{\alpha\alpha'}_{\boldsymbol{k},\sigma\sigma'}(i\omega_n) = -\frac{J_\alpha}{2}\frac{1}{i\omega_n-\xi_{\boldsymbol{k}\alpha}}\int_0^\beta d\tau\, e^{i\omega_n\tau} \times \sum_{\sigma''}\int\frac{d\boldsymbol{q}}{(2\pi)^3}\sigma^\mu_{\sigma\sigma''}\Phi^{\alpha\alpha'}_{\mu,\sigma''\sigma'}(\tau;\boldsymbol{k}+\boldsymbol{q}\tau,-\boldsymbol{k}0). \quad \text{(E7)}$$

Within the mean-field theory, the right-hand side of Eq. (E5) can be decoupled as

$$\sum_{\sigma''}\int\frac{d\boldsymbol{q}}{(2\pi)^3}\sigma^\mu_{\sigma\sigma''}\Phi^{\alpha\alpha'}_{\mu,\sigma''\sigma'}(\tau;\boldsymbol{k}+\boldsymbol{q}\tau,-\boldsymbol{k}0) \simeq -\frac{2V^*W}{J_\alpha}\epsilon_{\sigma\sigma'}\epsilon_{\alpha\alpha'}\frac{1}{\beta}\sum_n\frac{s_\alpha(i\omega_n-\xi_{\boldsymbol{k}\alpha})}{\bar{D}_{\boldsymbol{k}}(s_\alpha i\omega_n)}e^{-i\omega_n\tau}. \quad \text{(E8)}$$

Therefore we have reproduced Eq. (E1) from the equation of motion of the Cooper pair amplitude. Considering high-energy properties of the energy dispersion such as the presence of the band cutoff, the Cooper pair amplitude is secondarily induced owing to the presence of the composite pair amplitude, which is the primary order parameter breaking U(1) gauge symmetry.

APPENDIX F: MEISSNER RESPONSE

In this section, we consider the electromagnetic response in the superconducting state. Generally, we can rewrite the electromagnetic kernel in terms of the Green's function as follows:

$$K^p_{\mu\nu}(\boldsymbol{q},\nu_m) = e^2\int\frac{d\boldsymbol{k}}{(2\pi)^3}\frac{1}{\beta}\sum_{n=-\infty}^{\infty}\sum_{\alpha\alpha'}\sum_{\sigma\sigma'} \times\left[v^\mu_{\boldsymbol{k}\alpha}v^\nu_{\boldsymbol{k}\alpha'}\tilde{\mathcal{G}}^{\alpha\alpha'}_{\boldsymbol{k}_+,\sigma\sigma'}(i\omega_n+i\nu_m)\tilde{\mathcal{G}}^{\alpha\alpha'}_{\boldsymbol{k}_-,\sigma\sigma'}(i\omega_n) - v^\mu_{\boldsymbol{k}\alpha}v^\nu_{-\boldsymbol{k}\alpha'}\tilde{\mathcal{F}}^{\alpha\alpha'}_{\boldsymbol{k}_+,\sigma\sigma'}(i\omega_n+i\nu_m)\tilde{\mathcal{F}}^{\dagger\alpha\alpha'}_{\boldsymbol{k}_-,\sigma\sigma'}(i\omega_n)\right], \quad \text{(F1)}$$

$$K^d_{\mu\nu}(\boldsymbol{q},\nu_m) = \delta_{\mu\nu}\delta_{m0}e^2\int\frac{d\boldsymbol{k}}{(2\pi)^3}\sum_{\alpha,\sigma}\frac{\partial v^\mu_{\boldsymbol{k}\alpha}}{\partial k_\mu}\frac{1}{\beta}\sum_{n=-\infty}^{\infty}\tilde{\mathcal{G}}^{\alpha\alpha}_{\boldsymbol{k},\sigma\sigma}(i\omega_n), \quad \text{(F2)}$$

where $v^\mu_{\boldsymbol{k}\alpha} = \partial\varepsilon_{\boldsymbol{k}\alpha}/\partial k_\mu$ denotes the velocity operator. $\boldsymbol{k}_\pm = \boldsymbol{k}\pm\boldsymbol{q}/2$. $\nu_m = 2\pi m/\beta$ is bosonic Matsubara frequency. $\tilde{\mathcal{G}}(z)$ represents the electron Green's function including influences of all orders of the lattice regularization. It is defined as follows:

$$\tilde{\mathcal{G}}^{-1}_{\boldsymbol{k}}(z) = \mathcal{G}^{-1}_{\boldsymbol{k}}(z) - \tilde{\Sigma}_{\boldsymbol{k}}(z), \quad \text{(F3)}$$

where $\mathcal{G}^{\alpha\alpha'}_{\boldsymbol{k},\sigma\sigma'}(i\omega_n) = \int_0^\beta d\tau\langle -T_\tau[\psi_{\boldsymbol{k}\alpha\sigma}(\tau)\psi^\dagger_{\boldsymbol{k}\alpha'\sigma'}(0)]\rangle e^{i\omega_n\tau}$ describes the electron Green's function in the low-energy effective theory. $\tilde{\Sigma}_{\boldsymbol{k}}(z)$ denotes a self-energy, which describes the contribution from the lattice regularization and is given as

$$\tilde{\Sigma}^{\alpha\alpha'}_{\boldsymbol{k},\sigma\sigma'}(z) = \delta_{\alpha\alpha'}\delta_{\sigma\sigma'}\frac{|V|^2|W|^2}{z^2}\mathcal{G}^{\bar{\alpha}\bar{\alpha}}_{\boldsymbol{k},\sigma\sigma}(z). \quad \text{(F4)}$$

We derive the relation on the partial derivative of the Green's function $\tilde{\mathcal{G}}$ by the analytical calculation. It is given as follows:

$$\frac{\partial}{\partial k_\mu}\tilde{\mathcal{G}}^{\alpha\alpha}_{\boldsymbol{k},\sigma\sigma}(z) = \left(\tilde{\mathcal{G}}^{\alpha\alpha}_{\boldsymbol{k},\sigma\sigma}(z)\right)^2 v^\mu_{\boldsymbol{k}\alpha} + \tilde{\mathcal{F}}^{\alpha\bar{\alpha}}_{\boldsymbol{k},\sigma\bar{\sigma}}(z)\tilde{\mathcal{F}}^{\dagger\alpha\bar{\alpha}}_{\boldsymbol{k},\sigma\bar{\sigma}}(z)v^\mu_{-\boldsymbol{k}\bar{\alpha}}. \quad \text{(F5)}$$

Therefore the diamagnetic term in the static limit $\boldsymbol{q}\to\boldsymbol{0}$ and $\nu_m = 0$ can be transformed by calculating the partial integration:

$$K^d_{\mu\nu}(\boldsymbol{q},0) = -\delta_{\mu\nu}e^2\int\frac{d\boldsymbol{k}}{(2\pi)^3}\frac{1}{\beta}\sum_{m=-\infty}^{\infty}\sum_{\alpha,\sigma} \times\left[v^\mu_{\boldsymbol{k}\alpha}v^\mu_{\boldsymbol{k}\alpha}\left(\tilde{\mathcal{G}}^{\alpha\alpha}_{\boldsymbol{k},\sigma\sigma}(i\omega_m)\right)^2 + v^\mu_{\boldsymbol{k}\alpha}v^\mu_{-\boldsymbol{k}\bar{\alpha}}\tilde{\mathcal{F}}^{\alpha\bar{\alpha}}_{\boldsymbol{k},\sigma\bar{\sigma}}(i\omega_m)\tilde{\mathcal{F}}^{\dagger\alpha\bar{\alpha}}_{\boldsymbol{k},\sigma\bar{\sigma}}(i\omega_m)\right]. \quad \text{(F6)}$$

From above, the electromagnetic kernels in the static limit are given as follows:

$$K^p_{\mu\nu}(\boldsymbol{q},0) = +\tilde{K}_{\mu\nu} + \delta\tilde{K}_{\mu\nu}, \quad \text{(F7)}$$

$$K^d_{\mu\nu}(\boldsymbol{q},0) = -\tilde{K}_{\mu\nu} + \delta\tilde{K}_{\mu\nu}, \quad \text{(F8)}$$

where $\tilde{K}_{\mu\nu}$ and $\delta\tilde{K}_{\mu\nu}$ are defined as follows:

$$\tilde{K}_{\mu\nu} = \delta_{\mu\nu}e^2\int\frac{d\boldsymbol{k}}{(2\pi)^3}\frac{1}{\beta}\sum_{n=-\infty}^{\infty}\sum_{\alpha,\sigma}v^\mu_{\boldsymbol{k}\alpha}v^\nu_{\boldsymbol{k}\alpha}\left(\tilde{\mathcal{G}}^{\alpha\alpha}_{\boldsymbol{k},\sigma\sigma}(i\omega_n)\right)^2, \quad \text{(F9)}$$

$$\delta\tilde{K}_{\mu\nu} = -\delta_{\mu\nu}e^2\int\frac{d\boldsymbol{k}}{(2\pi)^3}\frac{1}{\beta}\sum_{n=-\infty}^{\infty}\sum_{\alpha,\sigma} \times v^\mu_{\boldsymbol{k}\alpha}v^\nu_{-\boldsymbol{k}\bar{\alpha}}\tilde{\mathcal{F}}^{\alpha\bar{\alpha}}_{\boldsymbol{k},\sigma\bar{\sigma}}(i\omega_n)\tilde{\mathcal{F}}^{\dagger\alpha\bar{\alpha}}_{\boldsymbol{k},\sigma\bar{\sigma}}(i\omega_n). \quad \text{(F10)}$$

The total electromagnetic kernel is given by $K_{\mu\nu} = 2\delta\tilde{K}_{\mu\nu}$. $\delta\tilde{K}_{\mu\nu}$ can be obtained as follows. First, we perform the summation for Matsubara frequencies of the anomalous Green's function:

$$\frac{1}{\beta}\sum_{n=-\infty}^{\infty}\tilde{\mathcal{F}}^{\alpha\bar{\alpha}}_{\boldsymbol{k},\sigma\bar{\sigma}}(i\omega_n)\tilde{\mathcal{F}}^{\dagger\alpha\bar{\alpha}}_{\boldsymbol{k},\sigma\bar{\sigma}}(i\omega_n) = \frac{1}{\beta}\sum_{n=-\infty}^{\infty}\sum_{\alpha'}\frac{|V_1|^2|V_2|^2}{E_c^2} \times\left(\frac{\theta(k_c-|\boldsymbol{k}-\boldsymbol{K}_{\alpha'}|)}{(i\omega_n-s_\alpha s_{\alpha'}E_{\boldsymbol{k}\alpha'+})(i\omega_n-s_\alpha s_{\alpha'}E_{\boldsymbol{k}\alpha'-})}\right)^2 = \sum_{\alpha'}\frac{2|V_1|^2|V_2|^2}{E_c^2}\frac{\theta(k_c-|\boldsymbol{k}-\boldsymbol{K}_{\alpha'}|)}{\left(\xi^2_{\boldsymbol{k}\alpha'}+4|V_{\alpha'}|^2\right)^{\frac{3}{2}}}. \quad \text{(F11)}$$

Therefore $\delta\tilde{K}_{\mu\nu}$ is given as

$$\delta\tilde{K}_{\mu\nu} = e^2 \sum_{\alpha} \int_{\boldsymbol{k}\in\mathcal{K}_\alpha} \frac{d\boldsymbol{k}}{(2\pi)^3} \frac{k_\mu k_\nu}{m_\alpha \tilde{m}_\alpha} \times \frac{8|V_1|^2|V_2|^2}{E_c^2} \frac{1}{\left(\xi_{\boldsymbol{k}\alpha}^2 + 4|V_\alpha|^2\right)^{\frac{3}{2}}} = \delta_{\mu\nu} \sum_{\alpha} \frac{2|V_1|^2|V_2|^2}{|V_\alpha|^2 E_c^2} \frac{n_\alpha e^2}{|\tilde{m}_\alpha|}, \tag{F12}$$

where we have used the relation $n_\alpha = (3/4)\rho_\alpha(0)|\mu_\alpha|$. Therefore we can obtain the electromagnetic kernel represented in Eq. (15).

APPENDIX G: EFFECT OF OVERLAPPING BETWEEN ELECTRON AND HOLE FERMI SURFACES

In this section, we study the effect of the overlapping between the semimetallic conduction bands by considering the Hamiltonian in Eq. (A4) with choosing $\xi_{\boldsymbol{k}1} = -\xi_{\boldsymbol{k}2} = \xi_{\boldsymbol{k}}$ and $|V| = |W|$. The Fermi surface structure in the normal state is schemtically illustrated in the inset of the lower panel of Fig. 4. Then, we obtain the energy dispersion, which is given by

$$E_{\boldsymbol{k}0} = \xi_{\boldsymbol{k}}, \tag{G1}$$

$$E_{\boldsymbol{k}\pm} = \frac{1}{2}\left(\xi_{\boldsymbol{k}} \pm \sqrt{\xi_{\boldsymbol{k}}^2 + 8|V|^2}\right). \tag{G2}$$

Therefore, even in the superconducting state, the density of states resulting from $E_{\boldsymbol{k}0}$ remains finite at the Fermi level and form a Bogoliubov-Fermi surface [44]. Since the self-consistent equation has the same form of that in Eq. (9), the stability of this gapless superconducting state is guaranteed when the Kondo coupling is antiferromagnetic. The results are consistent with the tight-binding calculation in Appendix D.

[1] F. Steglich, J. Aarts, C. D. Bredl, W. Lieke, D. Meschede, W. Franz, and H. Schäfer, Phys. Rev. Lett. **43**, 1892 (1979).
[2] D. Jërome, A. Mazaud, M. Ribault, and K. Bachgaard, J. Phys. Lett. **41**, 95 (1980).
[3] J. G. Bednorz and K. A. Müller, Z. Phys. B **64**, 189 (1986).
[4] For a review, see M. R. Norman, Science **332**, 196 (2011).
[5] H. R. Ott, H. Rudigier, Z. Fisk, and J. L. Smith, Phys. Rev. Lett. **50**, 1595 (1983).
[6] S. Kittaka, Y. Aoki, Y. Shimura, T. Sakakibara, S. Seiro, C. Geibel, F. Steglich, H. Ikeda, and K. Machida, Phys. Rev. Lett. **112**, 067002 (2014).
[7] Y. Shimizu, S. Kittaka, T. Sakakibara, Y. Haga, E. Yamamoto, H. Amitsuka, Y. Tsutsumi, and K. Machida, Phys. Rev. Lett. **114**, 147002 (2015).
[8] M. Hedo, Y. Inada, E. Yamamoto, Y. Haga, Y. Onuki, Y. Aoki, T. D. Matsuda, H. Sato, and S. Takahashi, J. Phys. Soc. Jpn. **67**, 272 (1998).
[9] N. F. Mott, Philos. Mag. **6**, 287 (1961).
[10] B. I. Halperin and T. M. Rice, Rev. Mod. Phys. **40**, 755 (1968).
[11] J. Kuneŝ, J. Phys. Condens. Matter **27**, 333201 (2015).
[12] V. J. Emery and S. Kivelson, Phys. Rev. B **46**, 10812 (1992).
[13] A. V. Balatsky and J. Bonĉa, Phys. Rev. B **48**, 7445 (1993).
[14] P. Coleman, E. Miranda, and A. Tsvelik, Phys. Rev. Lett. **70**, 2960 (1993).
[15] P. Coleman, E. Miranda, and A. Tsvelik, Phys. Rev. Lett. **74**, 1653 (1995).
[16] V. J. Emery and S. A. Kivelson, Phys. Rev. Lett. **71**, 3701 (1993).
[17] P. Coleman, A. M. Tsvelik, N. Andrei, and H. Y. Kee, Phys. Rev. B **60**, 3608 (1999).
[18] M. Jarrell, H. Pang, and D. L. Cox, Phys. Rev. Lett. **78**, 1996 (1997).
[19] F. B. Anders, Phys. Rev. B **66**, 020504(R) (2002).
[20] F. B. Anders, Eur. Phys. J. B **28**, 9 (2002).
[21] R. Flint, M. Dzero, and P. Coleman, Nat. Phys. **4**, 643 (2008).
[22] R. Flint and P. Coleman, Phys. Rev. Lett. **105**, 246404 (2010).
[23] R. Flint, A. H. Nevidomskyy, and P. Coleman, Phys. Rev. B **84**, 064514 (2011).
[24] S. Hoshino and Y. Kuramoto, Phys. Rev. Lett. **112**, 167204 (2014).
[25] For a recent review, see Y. Zhou, K. Kanoda, and T.-K. Ng, Rev. Mod. Phys. **89**, 025003 (2017).
[26] For a recent review, see L. Savary and L. Balents, Rep. Prog. Phys. **80**, 016502 (2017).
[27] D. L. Cox, Phys. Rev. Lett. **59**, 1240 (1987).
[28] D. L. Cox and A. Zawadowski, Adv. Phys. **47**, 599 (1998).
[29] S. Hoshino, Phys. Rev. B **90**, 115154 (2014).
[30] H. Kusunose, J. Phys. Soc. Jpn. **85**, 113701 (2016).
[31] G.-M. Zhang and L. Yu, Phys. Rev. B **62**, 76 (2000).
[32] S. Capponi and F. F. Assaad, Phys. Rev. B **63**, 155114 (2001).
[33] R. Kubo, J. Phys. Soc. Jpn. **12**, 570 (1957).
[34] A. Georges, G. Kotliar, W. Krauth, and M. J. Rozenberg, Rev. Mod. Phys. **68**, 13 (1996).
[35] A. Khurana, Phys. Rev. Lett. **64**, 1990 (1990).
[36] L. F. Mattheiss, Phys. Rev. B **8**, 3719 (1973).
[37] T. Onimaru, K. T. Matsumoto, Y. F. Inoue, K. Umeo, T. Sakakibara, Y. Karaki, M. Kubota, and T. Takabatake, Phys. Rev. Lett. **106**, 177001 (2011).
[38] T. L. Loucks and P. H. Cutler, Phys. Rev. **133**, A819 (1964).
[39] S. T. Inoue and J. Yamashita, J. Phys. Soc. Jpn. **35**, 677 (1973).
[40] Y. Yamane, T. Onimaru, K. Wakiya, K. T. Matsumoto, K. Umeo, and T. Takabatake, Phys. Rev. Lett. **121**, 077206 (2018).
[41] R. W. Stark and L. M. Falicov, Phys. Rev. Lett. **19**, 795 (1967).
[42] P. B. Allen, M. L. Cohen, L. M. Falicov, and R. V. Kasowski, Phys. Rev. Lett. **21**, 1794 (1968).
[43] S. Hoshino, J. Otsuki, and Y. Kuramoto, Phys. Rev. Lett. **107**, 247202 (2011).
[44] D. F. Agterberg, P. M. R. Brydon, and C. Timm, Phys. Rev. Lett. **118**, 127001 (2017).